Site-specific glycan analysis of the SARS-CoV-2 spike

Yasunori Watanabe[1,2,3#], Joel D. Allen[1#], Daniel Wrapp[4], Jason S. McLellan[4], Max Crispin[1*]

[1] School of Biological Sciences, University of Southampton, Southampton, SO17 1BJ, UK

[2] Oxford Glycobiology Institute, Department of Biochemistry, University of Oxford, South Parks Road, Oxford, OX1 3QU, UK

[3] Division of Structural Biology, University of Oxford, Wellcome Centre for Human Genetics, Oxford, OX3 7BN, UK

[4] Department of Molecular Biosciences, The University of Texas at Austin, Austin, TX 78712, USA

[#] These authors contributed to this work equally.

[*] To whom correspondence may be addressed. Email: max.crispin@soton.ac.uk

Abstract

The emergence of the betacoronavirus, SARS-CoV-2, the causative agent of COVID-19, represents a significant threat to global human health. Vaccine development is focused on the principal target of the humoral immune response, the spike (S) glycoprotein, which mediates cell entry and membrane fusion. SARS-CoV-2 S gene encodes 22 N-linked glycan sequons per protomer, which likely play a role in protein folding and immune evasion. Here, using a site-specific mass spectrometric approach, we reveal the glycan structures on a recombinant SARS-CoV-2 S immunogen. This analysis enables mapping of the glycan-processing states across the trimeric viral spike. We show how SARS-CoV-2 S glycans differ from typical host glycan processing, which may have implications in viral pathobiology and vaccine design.

Severe acute respiratory syndrome coronavirus-2 (SARS-CoV-2), the causative pathogen of COVID-19 (*1*, *2*), induces fever, severe respiratory illness and pneumonia. SARS-CoV-2 utilizes an extensively glycosylated spike (S) protein that protrudes from the viral surface to bind to angiotensin-converting enzyme 2 (ACE2) to mediate host-cell entry (*3*). The S protein is trimeric class I fusion protein, composed of two functional subunits, responsible for receptor binding (S1 subunit) and membrane fusion (S2 subunit) (*4*, *5*). Remarkably, the surface of the envelope spike is dominated by host-derived glycans with each trimer displaying 66 N-linked glycosylation sites. The S protein is a key target in vaccine design efforts (*6*), and understanding the glycosylation of recombinant viral spikes can reveal fundamental features of viral biology and guide vaccine design strategies (*7*, *8*).

Viral glycosylation has wide-ranging roles in viral pathobiology, including mediating protein folding and stability, and shaping viral tropism (*9*). Glycosylation sites are under selective pressure as they facilitate immune evasion by shielding specific epitopes from antibody neutralization. However, we note the low mutation rate of SARS-CoV-2, and as yet that there have been no observed mutations to N-linked glycosylation sites (*10*). Surfaces with an unusually high density of glycans can also enable immune recognition (*9*, *11*, *12*). The role of glycosylation in camouflaging immunogenic protein epitopes has been studied for other coronaviruses (*10*, *13*, *14*). Coronaviruses form virions by budding into the lumen of endoplasmic reticulum-Golgi intermediate compartments (ERGIC) (*15*, *16*). However, observations of complex-type glycans on virally derived material suggests that the viral glycoproteins are subjected to Golgi-resident processing enzymes (*13*, *17*).

High viral glycan density and local protein architecture can sterically impair the glycan maturation pathway. Impaired glycan maturation resulting in the presence of oligomannose-type glycans can be a sensitive reporter of native-like protein architecture (*8*), and site-specific glycan analysis can be used to compare different immunogens and monitor manufacturing processes (*18*). Additionally, glycosylation can influence the trafficking of recombinant immunogen to germinal centers (*19*).

To resolve the site-specific glycosylation of SARS-CoV-2 S protein and visualize the distribution of glycoforms across the protein surface, we expressed and purified three biological replicates of recombinant soluble material in an identical manner to that which was used to obtain the high-resolution cryo-electron microscopy (cryo-EM) structure, albeit without glycan processing blockade using kifunensine (*4*). This variant of the S protein

contains all 22 glycans on the SARS-CoV-2 S protein (**Figure 1A**). Stabilization of the trimeric prefusion structure was achieved using the "2P" stabilizing mutations (*20*) at residues 986 and 987, a "GSAS" substitution at the furin cleavage site (residues 682–685), and a C-terminal trimerization motif. This helps to maintain quaternary architecture during glycan processing. Prior to analysis, supernatant containing the recombinant SARS-CoV-2 S was purified by size-exclusion chromatography ensure only native-like trimeric protein was analyzed (**Figure 1B** and **Sup Fig. 1**). The trimeric conformation of the purified material was validated using negative-stain electron microscopy (**Figure 1C**).

To determine the site-specific glycosylation of SARS-CoV-2 S, we employed trypsin, chymotrypsin, and alpha-lytic protease to generate three glycopeptide samples. These proteases were selected to generate glycopeptides that contain a single N-linked glycan sequon. The glycopeptides were analyzed by liquid-chromatography-mass spectrometry (LC-MS), and the glycan compositions were determined for all 22 N-linked glycan sites (**Figure 2**). To convey the main processing features at each site, the abundances of each glycan are summed into oligomannose-, hybrid- and categories of complex-type glycosylation based on branching and fucosylation. The detailed, expanded graphs showing the diverse range of glycan compositions is presented in **Sup. Table 1** and **Sup. Fig. 2**.

There are two sites on SARS-CoV-2 S that are principally oligomannose-type: N234 and N709. The predominant oligomannose-type glycan structure observed across the protein, with the exception of N234, is $Man_5GlcNAc_2$, which demonstrates that these sites are largely accessible to α1,2-mannosidases but are poor substrates for GlcNAcT-I, which is the gateway enzyme in the formation of hybrid- and complex-type glycans in the Golgi apparatus. The stage at which processing is impeded is a signature related to the density and presentation of glycans on the viral spike. For example, the more densely glycosylated spikes of HIV-1 Env and Lassa virus GPC exhibit numerous sites dominated by $Man_9GlcNAc_2$ (*21–24*).

A mixture of oligomannose- and complex-type glycans can be found at sites N61, N122, N603, N717, N801 and N1074 (**Figure 2**). Of the 22 sites on the S protein, 8 contain significant populations of oligomannose-type glycans, highlighting how the processing of the SARS-CoV-2 S glycans is divergent from host glycoproteins (*25*). The remaining 14 sites are dominated by processed, complex-type glycans.

Although unoccupied glycosylation sites were detected on SARS-CoV-2 S, when quantified they were revealed to form a very minor component of the total peptide pool (**Sup.**

Table 2). In HIV-1 immunogen research, the holes generated by unoccupied glycan sites have been shown to be immunogenic and potentially give rise to distracting epitopes (*26*). The high occupancy of N-linked glycan sequons of SARS-CoV-2 S indicates that recombinant immunogens will not require further optimization to enhance site occupancy.

Using the cryo-EM structure of the trimeric SARS-CoV-2 S protein (PDB ID 6VSB) (*4*), we mapped the glycosylation status of the coronavirus spike mimetic onto the experimentally determined 3D structure (**Figure 3**). This combined mass spectrometric and cryo-EM analysis reveals how the N-linked glycans occlude distinct regions across the surface of the SARS-CoV-2 spike.

Shielding of the receptor binding sites on the SARS-CoV-2 spike by proximal glycosylation sites (N165, N234, N343) can be observed, especially when the receptor binding domain is in the "down" conformation. The shielding of receptor binding sites by glycans is a common feature of viral glycoproteins, as observed on SARS-CoV-1 S (*10*, *13*), HIV-1 Env (*27*), influenza HA (*28*, *29*), and LASV GPC (*24*). Given the functional constraints of receptor binding sites and the resulting low mutation rates of these residues, it is likely that there is selective pressure to utilize N-linked glycans to camouflage one of the most conserved and potentially vulnerable areas of their respective glycoproteins (*30*, *31*).

It is interesting to note the dispersion of oligomannose-type glycans across both the S1 and S2 subunits. This is in contrast to other viral glycoproteins, for example the dense glycan clusters in several strains of HIV-1 Env induce oligomannose-type glycans that are recognized by antibodies (*32*, *33*). In SARS-CoV-2 S the oligomannose-type structures are likely protected by the protein component, as exemplified by the N234 glycan which is partially sandwiched between the N-terminal and receptor-binding domains (**Figure 3**).

We characterized the N-linked glycans on extended flexible loop structures (N74 and N149) and at the membrane-proximal C-terminus (N1158, N1173, N1194) that were not resolved in the cryo-EM maps (*4*) These were determined to be complex-type glycans, consistent with steric accessibility of these residues.

Whilst the oligomannose-type glycan content (28%) (**Sup. Table 2**) is above that observed on typical host glycoproteins, it is lower than other viral glycoproteins. For example, one of the most densely glycosylated viral spike proteins is HIV-1 Env, which exhibits ~60% oligomannose-type glycans (*21*, *34*). This suggests that SARS-CoV-2 S protein is less densely glycosylated and that the glycans form less of a shield compared with other viral glycoproteins

including HIV-1 Env and LASV GPC, which may be beneficial for the elicitation of neutralizing antibodies.

Additionally, the processing of complex-type glycans is an important consideration in immunogen engineering, especially considering that epitopes of neutralizing antibodies against SARS-CoV-2 S can contain fucosylated glycans at N343 (*35*). Across the 22 N-linked glycosylation sites, 52% are fucosylated and 15% of the glycans contain at least one sialic acid residue (**Sup. Table 2** & **Sup. Fig. 3**). Our analysis reveals that N343 is highly fucosylated with 98% of detected glycans bearing fucose residues. Glycan modifications can be heavily influenced by the cellular expression system utilized. We have previously demonstrated for HIV-1 Env glycosylation that the processing of complex-type glycans is driven by the producer cell but that the levels of oligomannose-type glycans were largely independent of the expression system and is much more closely related to the protein structure and glycan density (*36*).

Highly dense glycan shields, such as those observed on LASV GPC and HIV-1 Env, feature so-called mannose clusters (*22*, *24*) on the protein surface (**Figure 4**). Whilst small mannose-type clusters have been characterized on the S1 subunit of Middle East respiratory syndrome (MERS) CoV S (*10*), no such phenomenon has been observed for SARS-CoV-1 or SARS-CoV-2 S proteins. The site-specific glycosylation analysis reported here suggests that the glycan shield of SARS-CoV-2 S is consistent with other coronaviruses and similarly exhibits numerous vulnerabilities throughout the glycan shield (*10*). Finally, we detected trace levels of O-linked glycosylation at T323/S325 with over 99% of these sites unmodified (**Sup. Fig. 4**) suggesting that O-linked glycosylation of this region is minimal when the structure is native-like.

Our glycosylation analysis of SARS-CoV-2 offers a detailed benchmark of site-specific glycan signatures characteristic of a natively folded trimeric spike. As an increasing number of glycoprotein-based vaccine candidates are being developed, their detailed glycan analysis offers a route for comparing immunogen integrity and will also be important to monitor as manufacturing processes are scaled for clinical use. Glycan profiling will therefore also be an important measure of antigen quality in the manufacture of serological testing kits. Finally, with the advent of nucleotide-based vaccines, it will be important to understand how those delivery mechanisms impact immunogen processing and presentation.

FIGURE LEGENDS

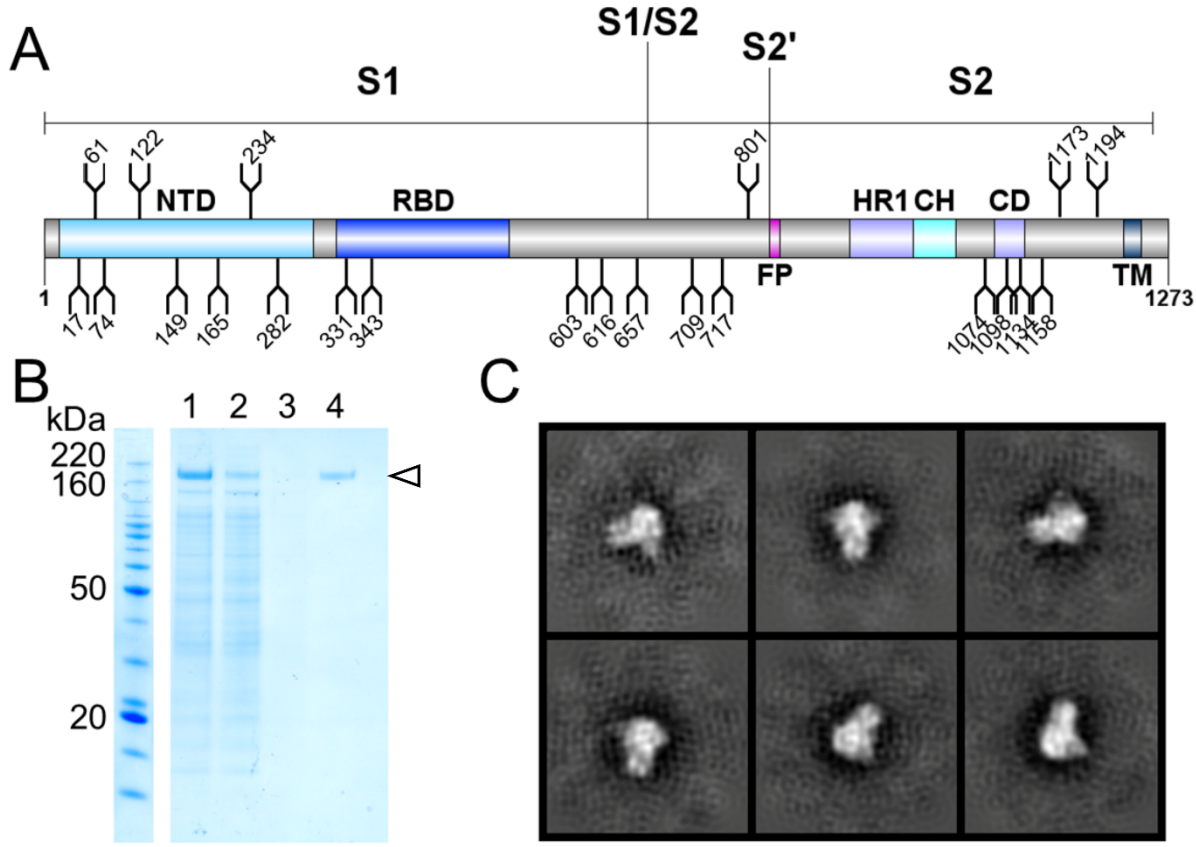

Figure 1. Expression and validation of SARS-CoV-2 S glycoprotein. (A) Schematic representation of SARS-CoV-2 S glycoprotein. The positions of N-linked glycosylation sequons (N-X-S/T, where X≠P) are shown as branches. Protein domains are illustrated: N-terminal domain (NTD), receptor-binding domain (RBD), fusion peptide (FP), heptad repeat 1 (HR1), central helix (CH), connector domain (CD), and transmembrane domain (TM). **(B)** SDS-PAGE analysis of SARS-CoV-2 S protein expressed in human embryonic kidney 293F cells. Lane 1: filtered supernatant from transfected cells; lane 2: flow-through from StrepTactin resin; lane 3: wash from StrepTactin resin; lane 4: elution from StrepTactin resin. **(C)** Negative-stain EM 2D class averages of the SARS-CoV-2 S protein. 2D class averages of the SARS-CoV-2 S protein are shown, confirming that the protein adopts the trimeric prefusion conformation matching the material used to determine the structure (*4*).

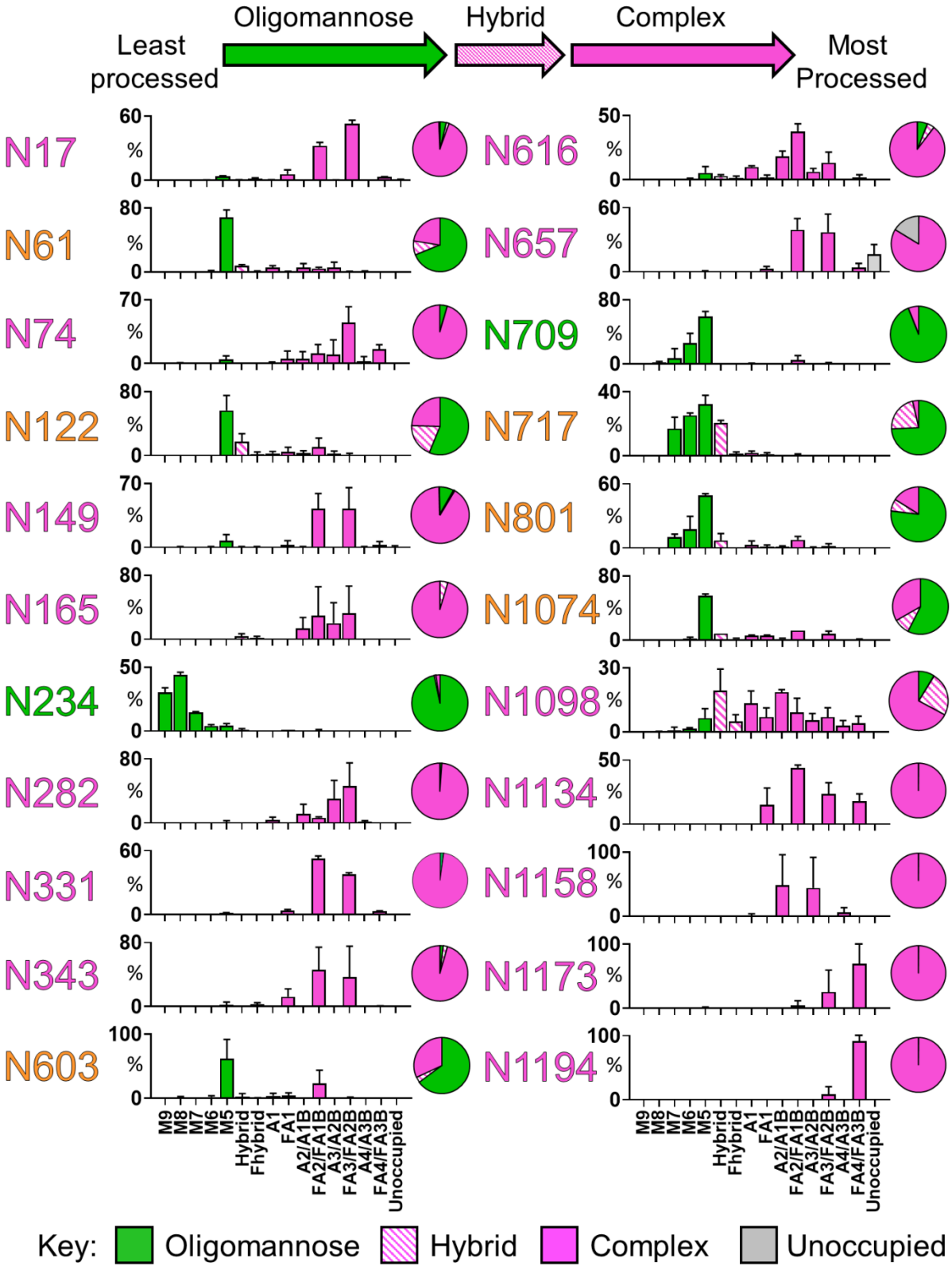

Figure 2: Site-specific N-linked glycosylation of SARS-CoV-2 S glycoprotein. The schematic illustrates the color code for the principal glycan types that can arise along the maturation pathway from oligomannose-, hybrid- to complex-type glycans. The graphs summarize quantitative mass spectrometric analysis of the glycan population present at

individual N-linked glycosylation sites simplified into categories of glycans. The oligomannose-type glycan series (M9 to M5; $Man_9GlcNAc_2$ to $Man_5GlcNAc_2$) is colored green, afucosylated and fucosylated hybrid-type glycans (Hybrid & F Hybrid) dashed pink, and complex glycans grouped according to the number of antennae and presence of core fucosylation (A1 to FA4) and are colored pink. Unoccupancy of an N-linked glycan site is represented in grey. The pie charts summarize the quantification of these glycans. Glycan sites are colored according to oligomannose-type glycan content with the glycan sites labelled in green (80−100%), orange (30−79%) and pink (0−29%). An extended version of the site-specific analysis showing the heterogeneity within each category can be found in **Sup. Table 1** and **Sup. Fig. 2**. The bar graphs represent the mean quantities of three biological replicates with error bars representing the standard error of the mean.

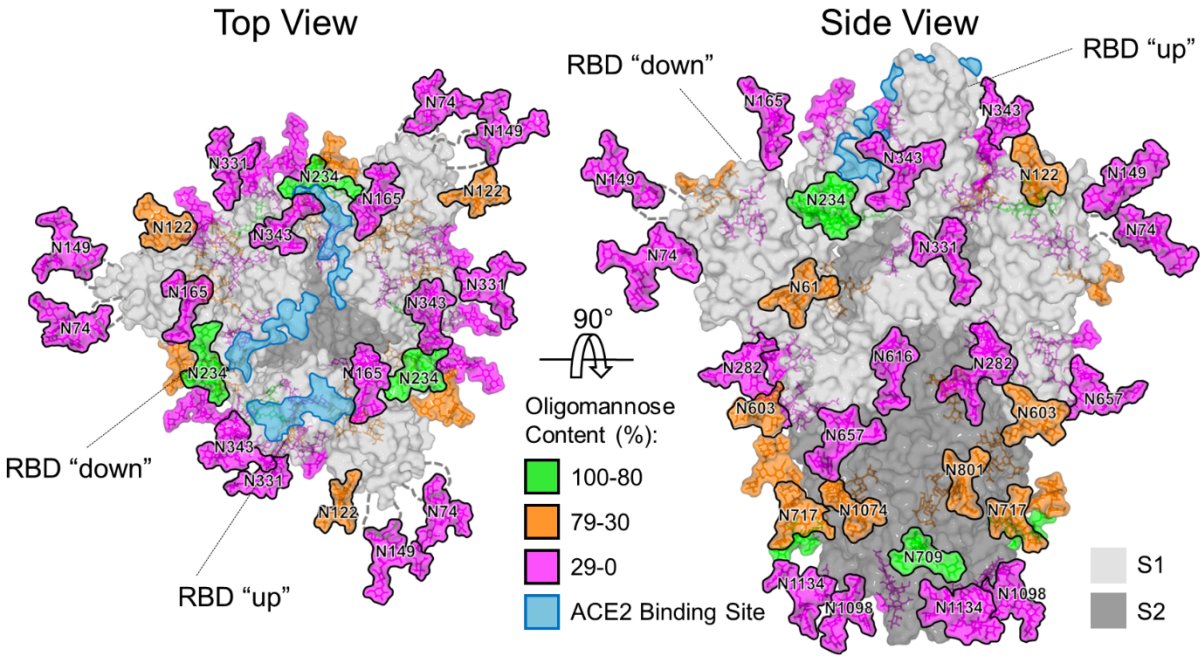

Figure 3. Structure-based mapping of SARS-CoV-2 S N-linked glycans. Representative glycans are modelled onto the prefusion structure of trimeric SARS-CoV-2 S glycoprotein (PDB ID 6VSB) (*4*), with one RBD in the "up" conformation and the other two RBDs in the "down" conformation. The glycans are colored according to oligomannose content as defined by the key. ACE2 receptor binding sites are highlighted in light blue. The S1 and S2 subunits are rendered with translucent surface representation, colored light and dark grey, respectively. Note that the flexible loops on which N74 and N149 glycan sites reside are represented as dashed lines with glycan sites on the loops mapped at their approximate regions.

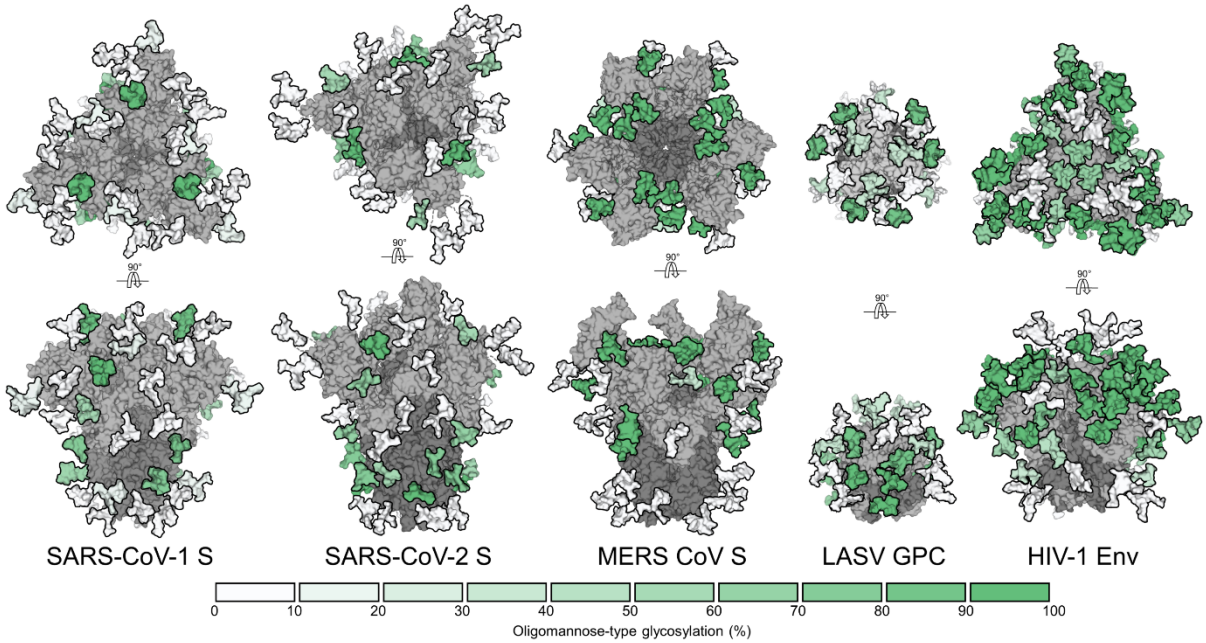

Figure 4. Under-processing of viral glycan shields. Left to Right: MERS-CoV S (*10*), SARS-CoV-1 S (*10*), SARS-CoV-2 S, LASV GPC (*24*), HIV-1 Env (*8*, *21*). Site-specific N-linked glycan oligomannose quantifications are colored according to the key. All glycoproteins were expressed as soluble trimers in HEK 293F cells apart from LASV GPC, which was derived from virus-like particles from Madin-Darby canine kidney II cells.

Acknowledgements

We thank M. Dixon and M. Gowland-Pryde for supporting our work on this project during the difficulties arising from the pandemic, and G. Ould for critical reading of the manuscript. **Funding:** This work was funded by the International AIDS Vaccine Initiative, Bill and Melinda Gates Foundation through the Collaboration for AIDS Vaccine Discovery (OPP1084519 to M.C., and 1196345 to M.C.), the NIAID (R01-AI127521 to J.S.M) and the Scripps Consortium for HIV Vaccine Development (CHAVD) (AI144462 to M.C.). M.C. is a Supernumerary Fellow of Oriel College, Oxford, and Professor Adjunct at Scripps Research, CA. **Author Contributions:** Y.W. and J.A. performed mass spectrometry experiments and analysed data. Y.W. built glycosylated models. Y.W., J.A., and D.W. expressed and purified proteins. Y.W., J.A., and M.C wrote the manuscript with input from all authors. **Competing interests:** J.S.M. is an inventor on U.S. patent application no. 62/412,703 ("Prefusion

Coronavirus Spike Proteins and Their Use"), and D.W., and J.S.M. are inventors on U.S. patent application no. 62/972,886 ("2019-nCoV Vaccine"). **Data and materials availability:** Mass spectrometry raw files have been deposited in the MassIVE proteomics database (doi:10.25345/C54X4K).

References

1. C. Huang *et al.*, *Lancet*. **6736**, 1–10 (2020).
2. X. Yang *et al.*, *Lancet Respir. Med.* (2020), doi:10.1016/S2213-2600(20)30079-5.
3. M. Letko, A. Marzi, V. Munster, *Nat. Microbiol.*, 1–8 (2020).
4. D. Wrapp *et al.*, *Science* (2020), doi:10.1126/science.abb2507.
5. A. C. Walls *et al.*, *Cell* (2020), doi:10.1016/j.cell.2020.02.058.
6. K. F. Amanat Fatima, *Cell*, 1–7 (2020).
7. L. Cao *et al.*, *Nat. Commun.* **8**, 14954 (2017).
8. A.-J. Behrens *et al.*, *J. Virol.* **91**, e01894-16 (2017).
9. Y. Watanabe, T. A. Bowden, I. A. Wilson, M. Crispin, *Biochim. Biophys. Acta*. **1863**, 1480–1497 (2019).
10. Y. Watanabe *et al.*, *bioRxiv*, in press, doi:10.1101/2020.02.20.957472.
11. M. Dalziel, M. Crispin, C. N. Scanlan, N. Zitzmann, R. A. Dwek, Emerging principles for the therapeutic exploitation of glycosylation. *Science*. **343** (2014), , doi:10.1126/science.1235681.
12. C. N. Scanlan, J. Offer, N. Zitzmann, R. A. Dwek, *Nature*. **446**, 1038–1045 (2007).
13. A. C. Walls *et al.*, *Cell*. **176**, 1026-1-39.e5 (2019).
14. T. J. Yang *et al.*, *Proc. Natl. Acad. Sci. U. S. A.* **117**, 1438–1446 (2020).
15. S. Stertz *et al.*, *Virology*. **361**, 304–315 (2007).
16. P. Venkatagopalan, S. M. Daskalova, L. A. Lopez, K. A. Dolezal, B. G. Hogue, *Virology*. **478**, 75–85 (2015).
17. G. Ritchie *et al.*, *Virology*. **399**, 257–69 (2010).
18. A. A. Hargett, M. B. Renfrow, Glycosylation of viral surface proteins probed by mass spectrometry. *Curr. Opin. Virol.* **36** (2019), pp. 56–66.
19. T. Tokatlian *et al.*, *Science*. **363**, 649–654 (2019).
20. J. Pallesen *et al.*, *Proc. Natl. Acad. Sci. U. S. A.* **114**, E7348–E7357 (2017).

21. W. B. Struwe *et al.*, *Cell Rep.* **24**, 1958-1966.e5 (2018).

22. A.-J. Behrens *et al.*, *Cell Rep.* **14**, 2695–2706 (2016).

23. M. Panico *et al.*, *Sci. Rep.* **6**, 32956 (2016).

24. Y. Watanabe *et al.*, *Proc. Natl. Acad. Sci.* **115**, 7320–7325 (2018).

25. I. Loke, D. Kolarich, N. H. Packer, M. Thaysen-Andersen, *Mol. Aspects Med.* **51**, 31–55 (2016).

26. M. Bianchi *et al.*, *Immunity*. **49**, 288-300.e8 (2018).

27. J. Jardine *et al.*, *Science*. **340**, 711–716 (2013).

28. C.-J. Wei *et al.*, *Sci. Transl. Med.* **2**, 24ra21 (2010).

29. R. Xu *et al.*, *Science*. **328**, 357–360 (2010).

30. X. Wei *et al.*, *Nature*. **422**, 307–312 (2003).

31. M. Zhang *et al.*, *Glycobiology*. **14**, 1229–1246 (2004).

32. G. B. E. Stewart-Jones *et al.*, *Cell*. **165**, 813–26 (2016).

33. D. Sok *et al.*, *Sci. Transl. Med.* **6**, 236ra63 (2014).

34. L. Cao *et al.*, *Nat. Commun.* **9**, 3693 (2018).

35. D. Pinto *et al.*, *bioRxiv*, in press, doi:10.1101/2020.04.07.023903.

36. L. K. Pritchard, D. J. Harvey, C. Bonomelli, M. Crispin, K. J. Doores, *J. Virol.* **89**, 8932–44 (2015).

Supplementary Information for:

Site-specific glycan analysis of the SARS-CoV-2 spike

Yasunori Watanabe[1,2,3#], Joel D. Allen[1#], Daniel Wrapp[4], Jason S. McLellan[4], Max Crispin[1*]

[1] School of Biological Sciences, University of Southampton, Southampton, SO17 1BJ, UK

[2] Oxford Glycobiology Institute, Department of Biochemistry, University of Oxford, South Parks Road, Oxford OX1 3QU, UK

[3] Division of Structural Biology, University of Oxford, Wellcome Centre for Human Genetics, Oxford, OX3 7BN, UK

[4] Department of Molecular Biosciences, The University of Texas at Austin, Austin, TX 78712, USA

[#] These authors contributed to this work equally.

[*]To whom correspondence may be addressed. Email: max.crispin@soton.ac.uk

This document includes:

Materials and Methods

Protein expression and purification

To express the prefusion S ectodomain, a gene encoding residues 1−1208 of SARS-CoV-2 S (GenBank: MN908947) with proline substitutions at residues 986 and 987, a "GSAS" substitution at the furin cleavage site (residues 682–685), a C-terminal T4 fibritin trimerization motif, an HRV3C protease cleavage site, a TwinStrepTag and an 8XHisTag was synthesized and cloned into the mammalian expression vector pαH. This expression vector was used to transiently transfect FreeStyle293F cells (Thermo Fisher) using polyethylenimine. Protein was purified from filtered cell supernatants using StrepTactin resin (IBA) or nickel-affinity chromatography before being subjected to additional purification by size-exclusion chromatography using a Superose 6 10/300 column (GE Healthcare) in 2 mM Tris pH 8.0, 200 mM NaCl and 0.02% NaN_3.

Negative-stain electron microscopy and 2D class averaging

Purified SARS-CoV-2 spike was diluted to a concentration of 0.04 mg/mL using 2 mM Tris pH 8.0, 200 mM NaCl and 0.02% NaN_3 before being applied to a plasma cleaned CF400-Cu grid (Electron Microscopy Sciences). Protein was then stained using methylamine tungstate (Nanoprobes) before being allowed to dry at room temperature for 15 minutes. This grid was imaged in a Talos TEM (Thermo Fisher Scientific) equipped with a Ceta 16M detector. Micrographs were collected using TIA v4.14 software at a nominal magnification of 92,000×, corresponding to a calibrated pixel size of 1.63 Å/pix. CTF estimation, particle picking and 2D class averaging were performed using *cis*TEM (*37*).

Glycopeptide analysis by mass spectrometry

Three 30 μg aliquots of SARS-CoV-2 S protein, from three biological replicates, were denatured for 1h in 50 mM Tris/HCl, pH 8.0 containing 6 M of urea and 5 mM dithiothreitol (DTT). Next, the S protein were reduced and alkylated by adding 20 mM iodoacetamide (IAA) and incubated for 1h in the dark, followed by a 1h incubation with 20 mM DTT to eliminate residual IAA. The alkylated Env proteins were buffer-exchanged into 50 mM Tris/HCl, pH 8.0 using Vivaspin columns (3 kDa) and digested separately overnight using trypsin chymotrypsin or alpha lytic protease (Mass Spectrometry Grade, Promega) at a ratio of 1:30 (w/w). The next day, the peptides were dried and extracted using C18 Zip-tip (MerckMilipore). The peptides were dried again, re-suspended in 0.1% formic acid and analyzed by nanoLC-ESI MS with an

Easy-nLC 1200 (Thermo Fisher Scientific) system coupled to a Fusion mass spectrometer (Thermo Fisher Scientific) using higher energy collision-induced dissociation (HCD) fragmentation. Peptides were separated using an EasySpray PepMap RSLC C18 column (75 µm × 75 cm). A trapping column (PepMap 100 C18 3µM 75µM x 2cm) was used in line with the LC prior to separation with the analytical column. The LC conditions were as follows: 275 minute linear gradient consisting of 0-32% acetonitrile in 0.1% formic acid over 240 minutes followed by 35 minutes of 80% acetonitrile in 0.1% formic acid. The flow rate was set to 200 nL/min. The spray voltage was set to 2.7 kV and the temperature of the heated capillary was set to 40 °C. The ion transfer tube temperature was set to 275 °C. The scan range was 400−1600 m/z. The HCD collision energy was set to 50%, appropriate for fragmentation of glycopeptide ions. Precursor and fragment detection were performed using an Orbitrap at a resolution MS^1= 100,000. MS^2= 30,000. The AGC target for MS^1=$4e^5$ and MS^2=$5e^4$ and injection time: MS^1=50ms MS^2=54ms.

Glycopeptide fragmentation data were extracted from the raw file using Byonic™ (Version 3.5) and Byologic™ software (Version 3.5; Protein Metrics Inc.). The glycopeptide fragmentation data were evaluated manually for each glycopeptide; the peptide was scored as true-positive when the correct b and y fragment ions were observed along with oxonium ions corresponding to the glycan identified. The MS data was searched using the Protein Metrics N-glycan library. The relative amounts of each glycan at each site as well as the unoccupied proportion were determined by comparing the extracted chromatographic areas for different glycotypes with an identical peptide sequence. All charge states for a single glycopeptide were summed. The precursor mass tolerance was set at 4 ppm and 10 ppm for fragments. A 1% false discovery rate (FDR) was applied. The relative amounts of each glycan at each site as well as the unoccupied proportion were determined by comparing the extracted ion chromatographic areas for different glycopeptides with an identical peptide sequence. Glycans were categorized according to the composition detected. HexNAc(2)Hex(9−5) was classified as M9 to M5. HexNAc(3)Hex(5−6)X was classified as Hybrid with HexNAc(3)Fuc(1)X classified as Fhybrid. Complex-type glycans were classified according to the number of processed antenna and fucosylation. If all of the following compositions have a fucose they are assigned into the FA categories. HexNAc(3)Hex(3-4)X is assigned as A1, HexNAc(4)X is A2/A1B, HexNAc(5)X is A3/A2B, and HexNAc(6)X is A4/A3B. As this fragmentation method does not provide linkage information compositional isomers are group, so for example a triantennary glycan contains HexNAc 5 but so does a biantennary glycans with a bisect. Any glycan

containing at least one sialic acid was counted as sialylated. The quantifications of glycan compositions were represented as the mean of three biological replicates +/- standard error of the mean.

For O-linked glycan analysis, trypsin and alpha lytic protease-generated glycopeptides were treated with PNGase F prior to analysis to remove N-linked glycans. This was performed on a single biological replicate using an HCD energy of 27%. The MS data was searched using the Protein Metrics 70 common O-linked glycan library.

Model construction

Structural models of N-linked glycan presentation on SARS-CoV-2 were created using electron microscopy structures (PDB ID: 6VSB) along with complex-, hybrid-, and oligomannose-type N-linked glycans (PDB ID 4BYH, 4B7I, and 2WAH). The most dominant glycoform presented at each site was modelled on to the N-linked carbohydrate attachment sites in Coot (*38*).

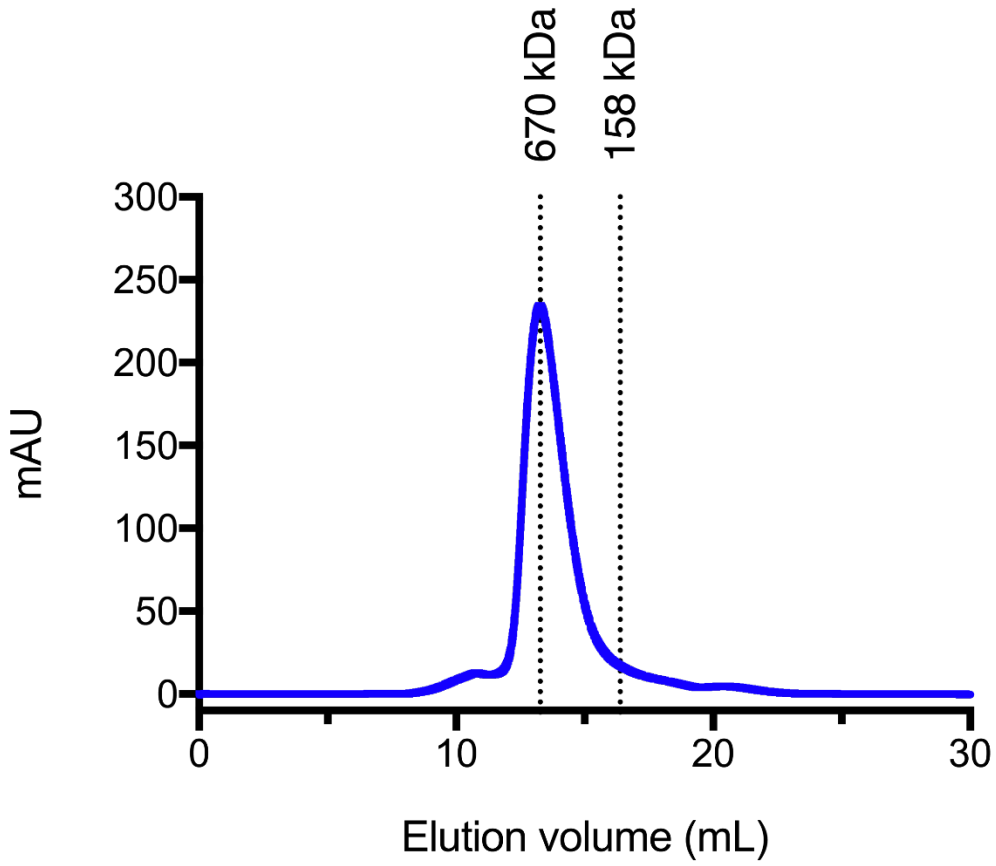

Supplementary Figure 1. Size-exclusion chromatogram of the affinity purified SARS-CoV-2 S protein. The elution volume of 670 kDa corresponding to the trimeric mass of the protein is shown.

Supplementary Table 1. Glycoform abundances observed across SARS CoV-2 S protein. The relative abundances of all N-linked glycans detected at each site is displayed. The displayed value is the mean percentage abundance of each glycan detected across three biological replicates. See also Figure 2.

	Glycan	17	61	74	122	149	165	234	282	331	343	603	616	657	709	717	801	1074	1098	1134	1158	1173	1194
1	HexNAc(2)Hex(9)	0	0	0	0	0	0	30	0	0	0	0	0	0	0	0	0	0	0	0	0	0	0
2	HexNAc(2)Hex(8)	0	0	0	0	0	0	44	0	0	0	1	0	0	2	0	0	0	0	0	0	0	0
3	HexNAc(2)Hex(7)	0	0	0	0	0	0	14	0	0	0	0	0	0	7	17	10	0	1	0	0	0	0
4	HexNAc(2)Hex(6)	1	1	0	0	0	0	4	0	0	0	2	1	0	26	25	17	2	2	0	0	0	0
5	HexNAc(2)Hex(5)	2	67	4	56	7	0	4	1	1	2	62	5	0	59	30	47	51	6	0	0	1	0
6	HexNAc(2)Hex(4)	0	1	0	0	0	0	0	0	0	0	0	0	0	0	2	2	5	0	0	0	0	0
7	HexNAc(2)Hex(4)Fuc(1)	0	0	0	0	0	0	0	0	0	0	0	0	0	0	0	0	0	0	0	0	0	0
8	HexNAc(3)Hex(5)	1	6	0	11	0	0	1	0	0	0	3	2	0	0	9	2	5	10	0	0	0	0
9	HexNAc(3)Hex(5)Fuc(1)	1	1	0	2	0	0	0	0	0	2	0	1	0	0	1	0	1	4	0	0	0	0
10	HexNAc(3)Hex(5)NeuAc(1)	1	1	0	3	0	0	0	0	0	0	0	0	0	0	1	2	0	2	0	0	0	0
11	HexNAc(3)Hex(6)	0	1	0	3	0	3	0	0	0	0	0	1	0	0	9	3	1	4	0	0	0	0
12	HexNAc(3)Hex(6)Fuc(1)	5	0	0	0	0	0	0	0	0	0	0	0	0	0	0	0	0	1	0	0	0	0
13	HexNAc(3)Hex(6)Fuc(1)NeuAc(1)	7	0	0	0	0	0	0	0	0	0	0	0	0	0	0	0	0	0	0	0	0	0
14	HexNAc(3)Hex(6)NeuAc(1)	1	0	0	1	0	0	0	0	0	0	0	0	0	0	2	0	1	3	0	0	0	0
15	HexNAc(2)Hex(3)	0	0	0	0	0	0	0	0	0	0	0	0	0	0	0	0	2	0	0	0	0	0
16	HexNAc(2)Hex(3)Fuc(1)	1	0	0	0	0	0	0	0	0	0	0	0	0	0	0	0	0	0	0	0	0	0
17	HexNAc(3)Hex(3)	3	4	1	3	0	1	0	3	0	0	0	5	0	0	0	3	2	4	0	0	0	0
18	HexNAc(3)Hex(3)Fuc(1)	5	0	3	2	3	0	0	0	3	8	3	1	3	0	0	1	3	4	7	0	0	0
19	HexNAc(3)Hex(4)	2	2	0	0	0	0	0	0	0	0	4	5	0	0	2	0	2	6	0	1	0	0
20	HexNAc(3)Hex(4)Fuc(1)	3	1	1	3	0	0	0	0	1	4	2	1	0	0	1	0	2	2	8	0	0	0
21	HexNAc(3)Hex(4)Fuc(1)NeuAc(1)	0	0	0	0	0	0	0	0	0	0	0	0	0	0	0	0	1	0	0	0	0	0
22	HexNAc(3)Hex(4)NeuAc(1)	0	0	0	0	0	0	0	0	0	0	0	0	0	0	0	0	0	3	0	0	0	0
23	HexNAc(4)Hex(3)	5	2	3	0	0	5	0	1	0	0	0	7	0	0	0	0	1	8	0	0	0	0
24	HexNAc(4)Hex(3)Fuc(1)	0	0	3	5	16	2	1	0	19	14	4	17	25	4	0	3	5	1	23	0	4	0
25	HexNAc(4)Hex(3)Fuc(2)	1	0	0	0	0	0	0	0	0	0	0	0	0	0	0	0	0	0	0	0	0	0
26	HexNAc(4)Hex(3)Fuc(3)	0	0	0	0	0	0	0	0	0	0	0	0	0	0	0	0	0	0	0	0	0	0
27	HexNAc(4)Hex(3)NeuAc(1)	0	0	0	0	0	0	0	0	0	0	0	0	0	0	0	0	0	0	0	0	0	0
28	HexNAc(4)Hex(4)	0	1	1	2	0	0	0	1	0	0	0	3	0	0	0	0	0	2	0	40	0	0
29	HexNAc(4)Hex(4)Fuc(1)	10	1	2	3	6	0	0	2	9	3	19	6	14	1	0	3	3	1	5	0	0	0
30	HexNAc(4)Hex(4)Fuc(1)NeuAc(1)	2	0	0	0	7	0	0	0	8	1	0	0	0	0	0	0	1	6	3	0	0	0
31	HexNAc(4)Hex(4)Fuc(2)	1	0	0	0	0	6	0	0	1	1	0	0	0	0	0	0	0	0	0	0	0	0
32	HexNAc(4)Hex(4)NeuAc(1)	0	1	0	0	0	0	0	0	0	0	0	0	0	0	0	0	0	6	0	0	0	0
33	HexNAc(4)Hex(5)	0	1	0	0	0	0	0	9	0	0	0	8	0	0	0	0	0	2	0	0	0	0
34	HexNAc(4)Hex(5)Fuc(1)	4	1	3	1	0	13	0	2	6	27	0	14	0	0	0	0	0	0	11	0	0	0
35	HexNAc(4)Hex(5)Fuc(1)NeuAc(1)	2	1	0	1	11	9	0	0	7	1	0	0	0	0	0	2	2	0	3	0	0	0
36	HexNAc(4)Hex(5)Fuc(1)NeuAc(2)	0	0	0	0	0	0	0	0	1	0	0	0	0	0	0	0	0	0	0	0	0	0
37	HexNAc(4)Hex(5)Fuc(2)	1	1	2	0	0	0	0	2	2	0	0	0	1	0	0	0	0	0	0	0	0	0
38	HexNAc(4)Hex(5)Fuc(2)NeuAc(1)	0	0	0	0	0	0	0	0	0	0	0	0	0	0	0	0	0	0	0	0	0	0
39	HexNAc(4)Hex(5)Fuc(3)	0	0	0	0	1	0	0	0	0	0	0	0	0	0	0	0	0	0	0	0	0	0
40	HexNAc(4)Hex(5)Fuc(3)NeuAc(1)	0	0	0	0	0	0	0	0	0	0	0	0	0	0	0	0	0	0	0	0	0	0
41	HexNAc(4)Hex(5)NeuAc(1)	0	1	0	1	0	9	0	0	0	0	0	0	0	0	0	0	0	1	0	1	0	0
42	HexNAc(4)Hex(5)NeuAc(2)	0	0	0	0	0	0	0	0	0	0	0	0	0	0	0	0	0	0	0	0	0	0
43	HexNAc(4)Hex(6)	0	0	0	0	0	0	0	0	0	0	0	0	0	0	0	0	0	0	0	3	0	0
44	HexNAc(4)Hex(6)Fuc(1)	0	0	0	0	0	0	0	0	0	0	0	0	0	0	0	0	0	0	0	0	0	0
45	HexNAc(4)Hex(6)Fuc(1)NeuAc(1)	0	0	0	0	0	0	0	0	0	0	0	0	0	0	0	0	0	0	0	0	0	0
46	HexNAc(4)Hex(6)Fuc(2)	0	0	0	0	0	0	0	0	0	0	0	0	0	0	0	0	0	0	0	0	0	0
47	HexNAc(4)Hex(6)Fuc(3)	0	0	0	0	0	0	0	0	0	0	0	0	0	0	0	0	0	0	0	0	0	0
48	HexNAc(4)Hex(6)NeuAc(1)	0	0	0	0	0	0	0	0	0	0	0	0	0	0	0	0	0	0	0	5	0	0
49	HexNAc(5)Hex(3)	0	3	3	2	0	16	0	7	0	0	0	3	0	0	0	0	0	1	0	0	0	0
50	HexNAc(5)Hex(3)Fuc(1)	7	0	3	1	6	0	0	21	16	23	1	1	11	1	0	2	6	3	12	0	25	0
51	HexNAc(5)Hex(3)Fuc(1)NeuAc(1)	7	0	0	0	9	0	0	0	1	0	0	0	0	0	0	0	0	0	0	0	0	0
52	HexNAc(5)Hex(4)	0	1	2	1	0	4	0	9	0	0	0	2	0	0	0	0	0	1	0	4	0	0
53	HexNAc(5)Hex(4)Fuc(1)	13	0	24	0	2	23	0	18	8	2	0	5	17	0	0	0	1	1	0	0	0	0
54	HexNAc(5)Hex(4)Fuc(1)NeuAc(1)	3	0	4	0	1	0	0	0	2	1	0	0	0	0	0	0	0	2	0	0	0	0
55	HexNAc(5)Hex(4)Fuc(1)NeuAc(2)	0	0	0	0	0	0	0	0	0	0	0	0	0	0	0	0	0	0	0	0	0	0
56	HexNAc(5)Hex(4)Fuc(2)	0	0	6	0	16	0	0	0	2	2	0	0	0	0	0	0	0	0	0	0	0	0
57	HexNAc(5)Hex(4)Fuc(2)NeuAc(1)	0	0	0	0	3	0	0	0	0	0	0	0	0	0	0	0	0	0	0	0	0	0
58	HexNAc(5)Hex(4)NeuAc(1)	0	0	2	0	0	0	0	2	0	0	0	0	0	0	0	0	0	1	0	0	0	0
59	HexNAc(5)Hex(4)NeuAc(2)	0	0	1	0	0	0	0	0	0	0	0	0	0	0	0	0	0	0	0	0	0	0
60	HexNAc(5)Hex(5)	0	2	1	0	0	0	0	0	0	0	0	0	0	0	0	0	0	0	0	7	0	0
61	HexNAc(5)Hex(5)Fuc(1)	2	0	3	0	5	10	0	7	5	8	0	1	6	0	0	0	0	0	0	0	0	0
62	HexNAc(5)Hex(5)Fuc(1)NeuAc(1)	0	0	1	0	0	0	0	0	1	0	0	0	0	0	0	0	1	0	0	0	0	0
63	HexNAc(5)Hex(5)Fuc(1)NeuAc(2)	0	0	0	0	0	0	0	0	0	0	0	0	0	0	0	0	0	1	0	0	8	0
64	HexNAc(5)Hex(5)Fuc(2)	0	0	0	0	0	0	0	0	0	0	0	0	0	0	0	0	0	0	0	0	0	0
65	HexNAc(5)Hex(5)Fuc(3)	0	0	0	0	0	0	0	0	0	0	0	0	0	0	0	0	0	0	0	0	0	0
66	HexNAc(5)Hex(5)NeuAc(1)	0	0	0	0	0	0	0	6	0	0	0	0	0	0	0	0	0	0	0	1	0	0
67	HexNAc(5)Hex(6)	0	0	0	0	0	0	0	0	0	0	0	1	0	0	0	0	0	0	0	0	0	0
68	HexNAc(5)Hex(6)Fuc(1)	0	0	1	0	0	0	0	0	2	0	0	6	0	0	0	0	0	0	10	0	0	0
69	HexNAc(5)Hex(6)Fuc(1)NeuAc(1)	0	0	0	0	0	0	0	0	0	0	0	0	1	0	0	0	0	0	0	0	0	0
70	HexNAc(5)Hex(6)Fuc(1)NeuAc(2)	0	0	2	0	0	0	0	0	0	0	0	0	1	0	0	0	0	0	0	0	0	0
71	HexNAc(5)Hex(6)Fuc(1)NeuAc(3)	0	0	0	0	0	0	0	0	0	0	0	0	0	0	0	0	0	0	0	0	0	0
72	HexNAc(5)Hex(6)Fuc(2)	0	0	0	0	0	0	0	0	0	0	0	0	0	0	0	0	0	0	0	0	0	0
73	HexNAc(5)Hex(6)Fuc(2)NeuAc(1)	0	0	0	0	0	0	0	0	0	0	0	0	0	0	0	0	0	0	0	0	0	0
74	HexNAc(5)Hex(6)Fuc(3)NeuAc(1)	0	0	0	0	0	0	0	0	0	0	0	0	0	0	0	0	0	0	0	0	0	0
75	HexNAc(5)Hex(6)NeuAc(1)	0	0	0	0	0	0	0	6	0	0	0	0	0	0	0	0	0	1	0	32	0	0
76	HexNAc(5)Hex(6)NeuAc(2)	0	0	0	0	0	0	0	0	0	0	0	0	0	0	0	0	0	0	0	0	0	0
77	HexNAc(6)Hex(3)	0	0	2	0	0	0	0	2	0	0	0	0	0	0	0	0	0	2	0	0	0	0
78	HexNAc(6)Hex(3)Fuc(1)	0	0	7	0	0	0	0	0	1	0	0	1	1	0	0	0	0	1	4	0	55	0
79	HexNAc(6)Hex(3)Fuc(1)NeuAc(1)	0	0	0	0	0	0	0	0	0	0	0	0	0	0	0	0	0	0	0	0	0	0
80	HexNAc(6)Hex(3)Fuc(2)	1	0	1	0	1	0	0	0	0	0	0	0	0	0	0	0	0	0	0	0	0	0
81	HexNAc(6)Hex(3)Fuc(3)	0	0	0	0	0	0	0	0	0	0	0	0	0	0	0	0	0	0	0	0	0	0
82	HexNAc(6)Hex(4)	0	0	1	0	0	0	0	0	0	0	0	0	0	0	0	0	0	0	0	0	0	0
83	HexNAc(6)Hex(4)Fuc(1)	1	0	0	0	0	0	0	0	1	0	0	0	0	0	0	0	0	0	0	0	4	0
84	HexNAc(6)Hex(4)Fuc(2)	0	0	0	0	0	0	0	0	0	0	0	0	0	0	0	0	0	0	0	0	0	0
85	HexNAc(6)Hex(4)NeuAc(1)	0	0	0	0	0	0	0	0	0	0	0	0	0	0	0	0	0	0	0	0	0	0
86	HexNAc(6)Hex(5)	0	0	0	0	0	0	0	0	0	0	0	0	0	0	0	0	0	0	0	2	0	0
87	HexNAc(6)Hex(5)Fuc(1)	0	0	4	0	0	0	0	0	1	0	0	0	3	0	0	0	0	0	6	0	0	0
88	HexNAc(6)Hex(5)Fuc(1)NeuAc(1)	0	0	0	0	0	0	0	0	0	0	0	0	0	0	0	0	0	0	0	0	0	50
89	HexNAc(6)Hex(5)Fuc(1)NeuAc(2)	0	0	4	0	0	0	0	0	0	0	0	0	0	0	0	0	0	0	0	0	0	0
90	HexNAc(6)Hex(5)Fuc(1)NeuAc(3)	0	0	0	0	0	0	0	0	0	0	0	0	0	0	0	0	0	0	0	0	0	42
91	HexNAc(6)Hex(5)Fuc(2)	0	0	0	0	0	0	0	0	0	0	0	0	0	0	0	0	0	0	0	0	0	0
92	HexNAc(6)Hex(6)	0	0	0	0	0	0	0	0	0	0	0	0	0	0	0	0	0	0	0	3	0	0
93	HexNAc(6)Hex(6)Fuc(1)	0	0	0	0	0	0	0	0	0	0	0	0	0	0	0	0	0	0	8	0	6	0
94	HexNAc(6)Hex(6)Fuc(1)NeuAc(1)	0	0	0	0	0	0	0	0	0	0	0	0	0	0	0	0	0	1	1	0	4	0
95	HexNAc(6)Hex(6)Fuc(1)NeuAc(2)	0	0	0	0	0	0	0	0	0	0	0	0	0	0	0	0	0	0	0	0	0	0
96	HexNAc(6)Hex(6)Fuc(2)	0	0	0	0	0	0	0	0	0	0	0	0	0	0	0	0	0	0	0	0	0	0
97	HexNAc(6)Hex(6)Fuc(3)	0	0	0	0	1	0	0	0	0	0	0	0	0	0	0	0	0	0	0	0	0	0
98	HexNAc(6)Hex(7)	0	0	0	0	0	0	0	0	0	0	0	0	0	0	0	0	0	0	0	0	0	0
99	HexNAc(6)Hex(7)Fuc(1)	0	0	0	0	0	0	0	0	0	0	0	1	0	0	0	0	0	0	0	0	0	0
100	HexNAc(6)Hex(7)Fuc(1)NeuAc(1)	0	0	0	0	0	0	0	0	0	0	0	0	0	0	0	0	0	1	0	0	0	0
101	HexNAc(6)Hex(7)Fuc(1)NeuAc(2)	0	0	0	0	0	0	0	0	0	0	0	0	0	0	0	0	0	0	0	0	0	0
102	HexNAc(6)Hex(7)Fuc(1)NeuAc(3)	0	0	0	0	0	0	0	0	0	0	0	0	0	0	0	0	0	0	0	0	0	0
103	HexNAc(6)Hex(7)Fuc(4)NeuAc(1)	0	0	0	0	0	0	0	0	0	0	0	0	0	0	0	0	0	0	0	0	0	0
104	HexNAc(6)Hex(7)NeuAc(1)	0	0	0	0	0	0	0	0	0	0	0	0	0	0	0	0	0	0	0	1	0	0
105	HexNAc(6)Hex(7)NeuAc(2)	0	0	0	0	0	0	0	0	0	0	0	0	0	0	0	0	0	0	0	0	0	0
106	HexNAc(6)Hex(7)NeuAc(4)	0	0	0	0	0	0	0	0	0	0	0	0	0	0	0	0	0	0	0	0	0	0
107	HexNAc(7)Hex(3)Fuc(1)	0	0	0	0	0	0	0	0	0	0	0	0	0	0	0	0	0	0	0	0	0	0
108	HexNAc(7)Hex(4)	0	0	0	0	0	0	0	0	0	0	0	0	0	0	0	0	0	0	0	0	0	0
109	HexNAc(7)Hex(4)Fuc(1)	0	0	0	0	0	0	0	0	0	0	0	0	0	0	0	0	0	0	0	0	0	0
110	Unoccupied	0	0	0	0	1	0	0	0	0	0	0	0	16	0	0	0	0	0	0	0	0	0

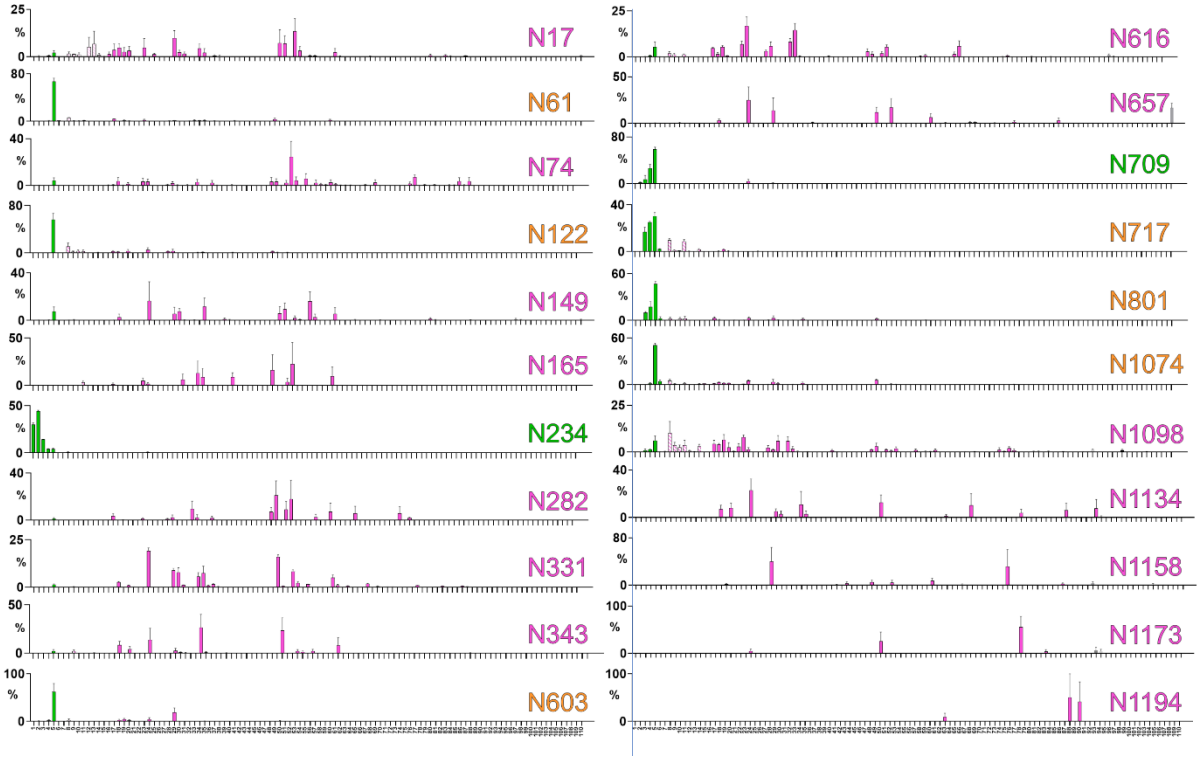

Supplementary Figure 2. Extended site-specific N-linked glycosylation of SARS-CoV-2 S glycoprotein. All glycan compositions detected across every N-linked glycan site are listed and numbered along the x-axis. The corresponding glycan compositions can be found in supplementary table 2. The bar graphs represent the mean abundance of each glycan of three biological repeats (+/- SEM) with oligomannose-type glycan series (green), hybrid glycans (dashed pink), and complex glycans (pink). Glycan sites are colored according to oligomannose-type glycan content with the glycan sites labelled in green (80−100%), orange (30−79%) and pink (0−29%). See also **Figure 2.**

Supplementary Table 2. Glycoform abundances observed across SARS CoV-2 S protein. The upper table shows the categorized glycan compositions at each N-linked glycan site with the reported value the mean of three biological replicates. The global averages are shown in the right-hand table. The lower table further categorizes the glycan compositions into oligomannose-, hybrid-, and complex-type as well as the percentage of glycan compositions containing at least one fucose or one sialic acid residue. See also Figure 2.

	N17	N61	N74	N122	N149	N165	N234	N282	N331	N343	N603	N616	N657	N709	N717	N801	N1074	N1098	N1134	N1158	N1173	N1194
M9	0	0	0	0	0	0	30	0	0	0	0	0	0	0	0	0	0	0	0	0	0	0
M8	0	0	0	0	0	0	44	0	0	0	1	0	0	2	0	0	0	0	0	0	0	0
M7	0	0	0	0	0	0	14	0	0	0	0	0	0	7	17	10	0	1	0	0	0	0
M6	0	1	0	0	0	0	4	0	0	0	2	1	0	26	25	17	2	2	0	0	0	0
M5	3	68	4	56	7	0	4	1	1	2	62	5	0	59	32	49	55	6	0	0	1	0
Hybrid	0	8	0	17	0	3	1	0	0	0	3	3	0	0	21	7	8	19	0	0	0	0
Fhybrid	2	1	0	2	0	1	0	0	0	2	0	1	0	0	1	0	1	5	0	0	0	0
A1	0	5	1	3	0	0	0	4	0	0	4	10	0	0	2	3	5	14	0	1	0	0
FA1	6	1	5	5	3	0	1	0	4	12	4	2	3	0	1	1	5	7	15	0	0	0
A2/A1B	0	6	5	3	0	14	0	11	0	0	0	18	0	0	0	1	2	19	0	48	0	0
FA2/FA1B	32	4	11	10	42	29	1	6	53	46	23	37	39	5	1	8	12	9	44	0	4	0
A3/A2B	0	6	10	3	0	20	0	30	0	0	0	6	0	0	0	0	0	5	0	44	0	0
FA3/FA2B	53	1	45	1	42	32	0	46	38	37	1	13	37	1	0	2	8	7	23	0	25	8
A4/A3B	0	0	3	0	0	0	0	2	0	0	0	0	0	0	0	0	0	3	0	6	0	0
FA4/FA3B	3	0	16	0	3	0	0	0	3	0	0	2	4	0	0	0	1	4	18	0	70	92
Unoccupied	1	0	0	0	1	0	0	0	0	0	0	0	16	0	0	0	0	0	0	0	0	0

Total	
M9	1
M8	2
M7	2
M6	4
M5	19
Hybrid	4
Fhybrid	1
A1	2
FA1	3
A2/A1B	6
FA2/FA1B	19
A3/A2B	6
FA3/FA2B	19
A4/A3B	1
FA4/FA3B	10
Unoccupied	1

%	N17	N61	N74	N122	N149	N165	N234	N282	N331	N343	N603	N616	N657	N709	N717	N801	N1074	N1098	N1134	N1158	N1173	N1194
Mannose	4	69	4	56	8	0	97	1	2	2	65	6	0	94	74	77	57	9	0	0	1	0
Hybrid	2	9	0	19	1	5	1	0	0	3	3	4	0	0	22	7	9	24	0	0	0	0
Complex	94	22	96	25	91	95	2	99	98	96	32	90	83	6	4	16	33	67	100	100	99	100
Unoccupied	1	0	0	0	1	0	0	0	0	0	0	0	16	0	0	0	0	0	0	0	0	0
Fucosylation	95	6	77	18	91	63	2	52	98	98	29	56	83	5	3	11	27	31	100	0	99	100
Sialylation	20	4	18	5	33	18	0	14	22	4	0	1	2	0	2	5	6	30	7	39	4	100

Total	
Mannose	28
Hybrid	5
Complex	66
Unoccupied	1
Fucosylation	52
Sialylation	15

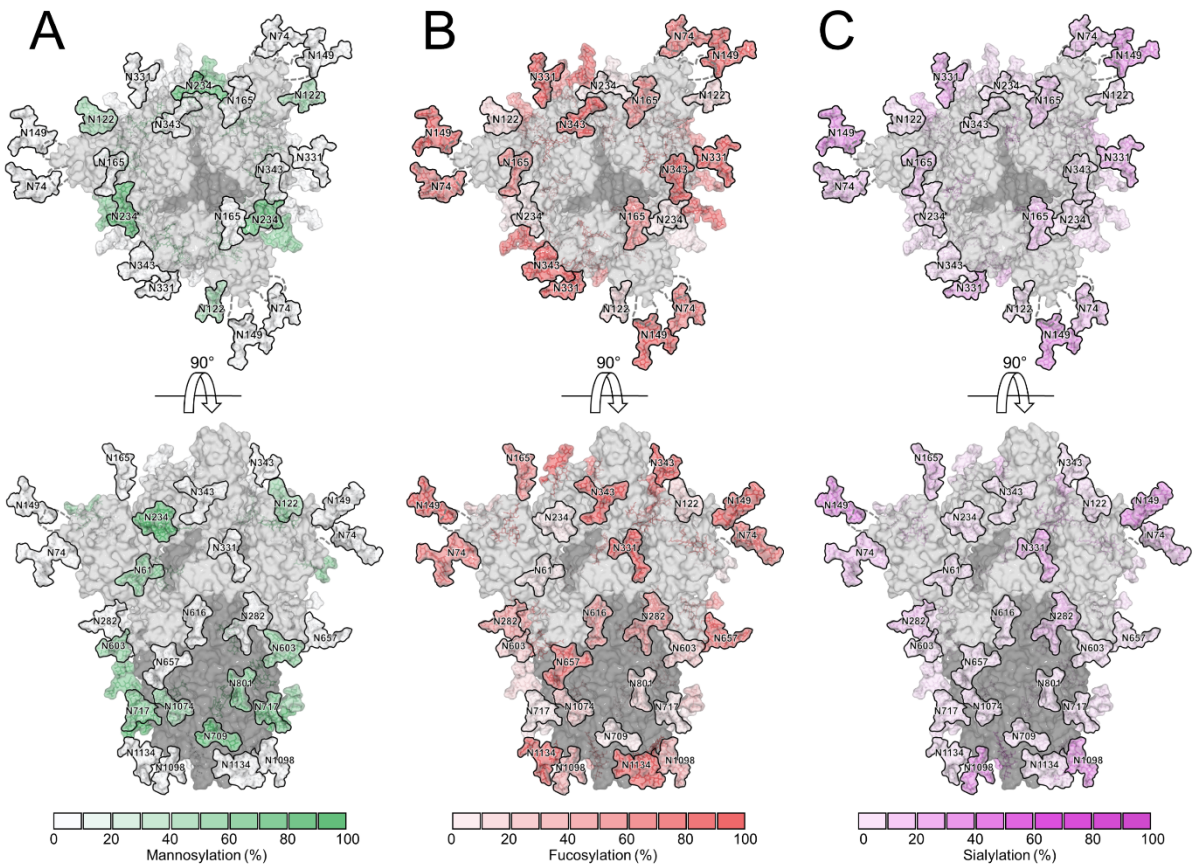

Supplementary Figure 3. Glycosylated model of SARS-CoV-2 S glycoprotein highlighting different glycan modifications. The experimentally determined quantities of mannosylation, fucosylation and sialylation presented in Supplementary Table 2 were used to color the glycosylated model of SARS-CoV2 S protein presented in Figure 3. Glycans are highlighted according to mannosylation **(A)**, fucosylation **(B)** and sialylation **(C)** levels as denoted in the keys. S1 and S2 subunits are colored light grey and dark grey, respectively.

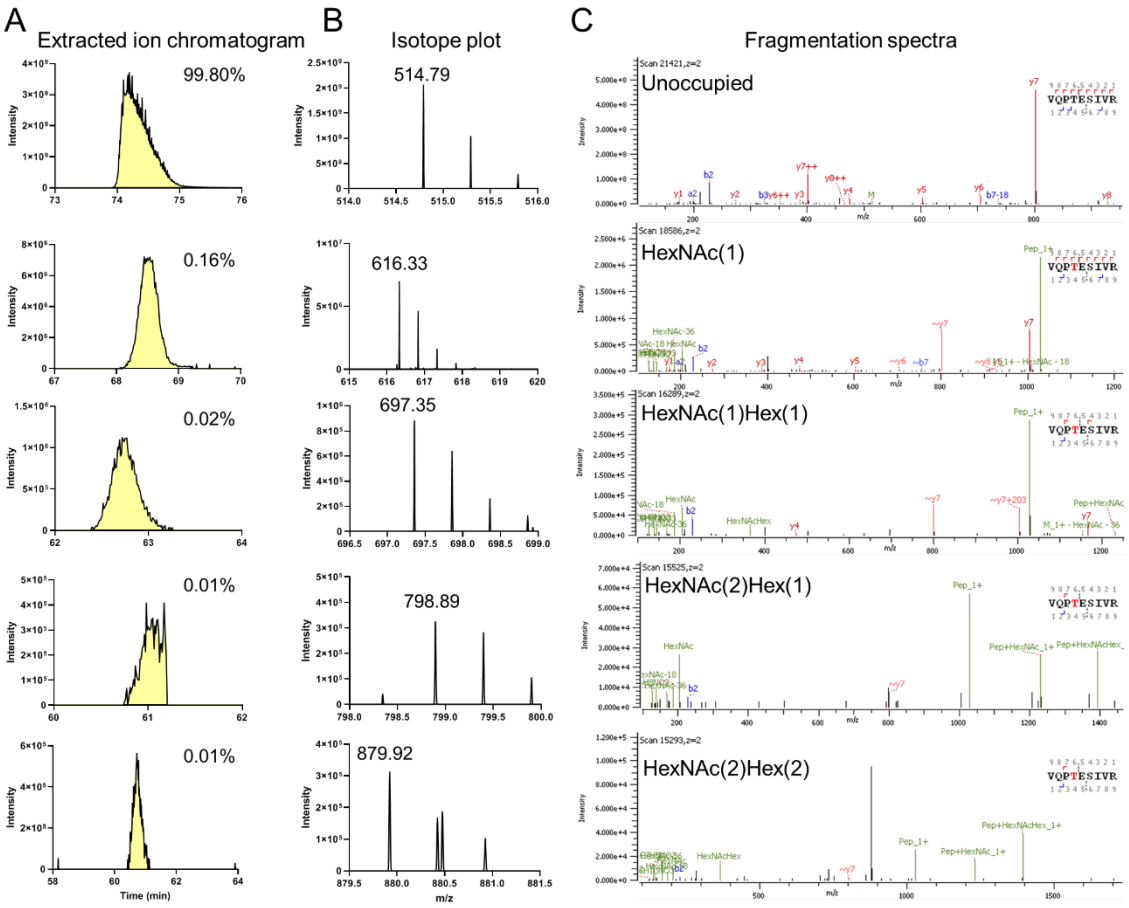

Supplementary Figure 4. Detection of low levels of mucin-type O-linked glycosylation at T323/S325 of SARS-CoV-2 S. O-linked glycan compositions were observed at T323/S325. This analysis was performed on a single biological replicate. For each peptide/glycopeptide detected the extracted ion chromatogram (XIC) (A), isotope distribution (B), and fragmentation spectrum (C) is shown. The monoisotopic peak *m/z* is labelled in (B). Fragment ions are colored blue and red for b- and y-ions, respectively. Oxonium ions are colored in green.

References

1. C. Huang, Y. Wang, X. Li, L. Ren, J. Zhao, Y. Hu, L. Zhang, G. Fan, J. Xu, X. Gu, Clinical features of patients infected with 2019 novel coronavirus in Wuhan , China. *Lancet*. **6736**, 1–10 (2020).

2. X. Yang, Y. Yu, J. Xu, H. Shu, J. Xia, H. Liu, Y. Wu, L. Zhang, Z. Yu, M. Fang, T. Yu, Y. Wang, S. Pan, X. Zou, S. Yuan, Y. Shang, Clinical course and outcomes of critically ill patients with SARS-CoV-2 pneumonia in Wuhan, China: a single-centered, retrospective, observational study. *Lancet Respir. Med.* (2020), doi:10.1016/S2213-2600(20)30079-5.

3. M. Letko, A. Marzi, V. Munster, Functional assessment of cell entry and receptor usage for SARS-CoV-2 and other lineage B betacoronaviruses. *Nat. Microbiol.*, 1–8 (2020).

4. D. Wrapp, N. Wang, K. S. Corbett, J. A. Goldsmith, C.-L. Hsieh, O. Abiona, B. S. Graham, J. S. McLellan, Cryo-EM structure of the 2019-nCoV spike in the prefusion conformation. *Science* (2020), doi:10.1126/science.abb2507.

5. A. C. Walls, Y.-J. Park, M. A. Tortorici, A. Wall, A. T. McGuire, D. Veesler, Structure, Function, and Antigenicity of the SARS-CoV-2 Spike Glycoprotein. *Cell* (2020), doi:10.1016/j.cell.2020.02.058.

6. K. F. Amanat Fatima, SARS-CoV-2 vaccines: status report. *Cell*, 1–7 (2020).

7. L. Cao, J. K. Diedrich, D. W. Kulp, M. Pauthner, L. He, S.-K. R. Park, D. Sok, C. Y. Su, C. M. Delahunty, S. Menis, R. Andrabi, J. Guenaga, E. Georgeson, M. Kubitz, Y. Adachi, D. R. Burton, W. R. Schief, J. R. Yates III, J. C. Paulson, Global site-specific N-glycosylation analysis of HIV envelope glycoprotein. *Nat. Commun.* **8**, 14954 (2017).

8. A.-J. Behrens, D. J. Harvey, E. Milne, A. Cupo, A. Kumar, N. Zitzmann, W. B. Struwe, J. P. Moore, M. Crispin, Molecular architecture of the cleavage-dependent mannose patch on a soluble HIV-1 envelope glycoprotein trimer. *J. Virol.* **91**, e01894-16 (2017).

9. Y. Watanabe, T. A. Bowden, I. A. Wilson, M. Crispin, Exploitation of glycosylation in enveloped virus pathobiology. *Biochim. Biophys. Acta*. **1863**, 1480–1497 (2019).

10. Y. Watanabe, Z. T. Berndsen, J. Raghwani, G. E. Seabright, J. D. Allen, J. S. McLellan, I. A. Wilson, T. A. Bowden, A. B. Ward, M. Crispin, *bioRxiv*, in press, doi:10.1101/2020.02.20.957472.

11. M. Dalziel, M. Crispin, C. N. Scanlan, N. Zitzmann, R. A. Dwek, Emerging principles for the therapeutic exploitation of glycosylation. *Science*. **343** (2014), , doi:10.1126/science.1235681.

12. C. N. Scanlan, J. Offer, N. Zitzmann, R. A. Dwek, Exploiting the defensive sugars of HIV-1 for drug and vaccine design. *Nature*. **446**, 1038–1045 (2007).

13. A. C. Walls, X. Xiong, Y.-J. Park, M. A. Tortorici, J. Snijder, J. Quispe, E. Cameroni,

R. Gopal, M. Dai, A. Lanzavecchia, M. Zambon, F. A. Rey, D. Corti, D. Veesler, Unexpected receptor functional mimicry elucidates activation of coronavirus fusion. *Cell*. **176**, 1026-1-39.e5 (2019).

14. T. J. Yang, Y. C. Chang, T. P. Ko, P. Draczkowski, Y. C. Chien, Y. C. Chang, K. P. Wu, K. H. Khoo, H. W. Chang, S. Te Danny Hsu, Cryo-EM analysis of a feline coronavirus spike protein reveals a unique structure and camouflaging glycans. *Proc. Natl. Acad. Sci. U. S. A.* **117**, 1438–1446 (2020).

15. S. Stertz, M. Reichelt, M. Spiegel, T. Kuri, L. Martínez-Sobrido, A. García-Sastre, F. Weber, G. Kochs, The intracellular sites of early replication and budding of SARS-coronavirus. *Virology*. **361**, 304–315 (2007).

16. P. Venkatagopalan, S. M. Daskalova, L. A. Lopez, K. A. Dolezal, B. G. Hogue, Coronavirus envelope (E) protein remains at the site of assembly. *Virology*. **478**, 75–85 (2015).

17. G. Ritchie, D. J. Harvey, F. Feldmann, U. Stroeher, H. Feldmann, L. Royle, R. A. Dwek, P. M. Rudd, Identification of N-linked carbohydrates from severe acute respiratory syndrome (SARS) spike glycoprotein. *Virology*. **399**, 257–69 (2010).

18. A. A. Hargett, M. B. Renfrow, Glycosylation of viral surface proteins probed by mass spectrometry. *Curr. Opin. Virol.* **36** (2019), pp. 56–66.

19. T. Tokatlian, B. J. Read, C. A. Jones, D. W. Kulp, S. Menis, J. Y. H. Chang, J. M. Steichen, S. Kumari, J. D. Allen, E. L. Dane, A. Liguori, M. Sangesland, D. Lingwood, M. Crispin, W. R. Schief, D. J. Irvine, Innate immune recognition of glycans targets HIV nanoparticle immunogens to germinal centers. *Science*. **363**, 649–654 (2019).

20. J. Pallesen, N. Wang, K. S. Corbett, D. Wrapp, R. N. Kirchdoerfer, H. L. Turner, C. A. Cottrell, M. M. Becker, L. Wang, W. Shi, W.-P. Kong, E. L. Andres, A. N. Kettenbach, M. R. Denison, J. D. Chappell, B. S. Graham, A. B. Ward, J. S. McLellan, Immunogenicity and structures of a rationally designed prefusion MERS-CoV spike antigen. *Proc. Natl. Acad. Sci. U. S. A.* **114**, E7348–E7357 (2017).

21. W. B. Struwe, E. Chertova, J. D. Allen, G. E. Seabright, Y. Watanabe, D. J. Harvey, M. Medina-Ramirez, J. D. Roser, R. Smith, D. Westcott, B. F. Keele, J. W. Bess, R.

W. Sanders, J. D. Lifson, J. P. Moore, M. Crispin, Site-specific glycosylation of virion-derived HIV-1 Env Is mimicked by a soluble trimeric immunogen. *Cell Rep.* **24**, 1958-1966.e5 (2018).

22. A.-J. Behrens, S. Vasiljevic, L. Pritchard, D. Harvey, R. Andev, S. Krumm, W. Struwe, A. Cupo, A. Kumar, N. Zitzmann, G. Seabright, H. Kramer, D. R. Spencer, L. Royle, J. Lee, P. Klasse, D. Burton, I. Wilson, A. Ward, R. Sanders, J. Moore, K. Doores, M. Crispin, Composition and antigenic effects of individual glycan sites of a trimeric HIV-1 envelope glycoprotein. *Cell Rep.* **14**, 2695–2706 (2016).

23. M. Panico, L. Bouché, D. Binet, M.-J. O'Connor, D. Rahman, P.-C. Pang, K. Canis, S. J. North, R. C. Desrosiers, E. Chertova, B. F. Keele, J. W. Bess, J. D. Lifson, S. M. Haslam, A. Dell, H. R. Morris, Mapping the complete glycoproteome of virion-derived HIV-1 gp120 provides insights into broadly neutralizing antibody binding. *Sci. Rep.* **6**, 32956 (2016).

24. Y. Watanabe, J. Raghwani, J. D. Allen, G. E. Seabright, S. Li, F. Moser, J. T. Huiskonen, T. Strecker, T. A. Bowden, M. Crispin, Structure of the Lassa virus glycan shield provides a model for immunological resistance. *Proc. Natl. Acad. Sci.* **115**, 7320–7325 (2018).

25. I. Loke, D. Kolarich, N. H. Packer, M. Thaysen-Andersen, Emerging roles of protein mannosylation in inflammation and infection. *Mol. Aspects Med.* **51**, 31–55 (2016).

26. M. Bianchi, H. L. Turner, B. Nogal, C. A. Cottrell, D. Oyen, M. Pauthner, R. Bastidas, R. Nedellec, L. E. McCoy, I. A. Wilson, D. R. Burton, A. B. Ward, L. Hangartner, Electron-Microscopy-Based Epitope Mapping Defines Specificities of Polyclonal Antibodies Elicited during HIV-1 BG505 Envelope Trimer Immunization. *Immunity*. **49**, 288-300.e8 (2018).

27. J. Jardine, J.-P. Julien, S. Menis, T. Ota, O. Kalyuzhniy, A. McGuire, D. Sok, P.-S. Huang, S. MacPherson, M. Jones, T. Nieusma, J. Mathison, D. Baker, A. B. Ward, D. R. Burton, L. Stamatatos, D. Nemazee, I. A. Wilson, W. R. Schief, Rational HIV immunogen design to target specific germline B cell receptors. *Science*. **340**, 711–716 (2013).

28. C.-J. Wei, J. C. Boyington, K. Dai, K. V. Houser, M. B. Pearce, W.-P. Kong, Z. -y. Yang, T. M. Tumpey, G. J. Nabel, Cross-neutralization of 1918 and 2009 Influenza

viruses: role of glycans in viral evolution and vaccine design. *Sci. Transl. Med.* **2**, 24ra21 (2010).

29. R. Xu, D. C. Ekiert, J. C. Krause, R. Hai, J. E. Crowe, I. A. Wilson, Structural basis of preexisting immunity to the 2009 H1N1 pandemic influenza virus. *Science*. **328**, 357–360 (2010).

30. X. Wei, J. M. Decker, S. Wang, H. Hui, J. C. Kappes, X. Wu, J. F. Salazar-Gonzalez, M. G. Salazar, J. M. Kilby, M. S. Saag, N. L. Komarova, M. A. Nowak, B. H. Hahn, P. D. Kwong, G. M. Shaw, Antibody neutralization and escape by HIV-1. *Nature*. **422**, 307–312 (2003).

31. M. Zhang, B. Gaschen, W. Blay, B. Foley, N. Haigwood, C. Kuiken, B. Korber, Tracking global patterns of N-linked glycosylation site variation in highly variable viral glycoproteins: HIV, SIV, and HCV envelopes and influenza hemagglutinin. *Glycobiology*. **14**, 1229–1246 (2004).

32. G. B. E. Stewart-Jones, C. Soto, T. Lemmin, G.-Y. Chuang, A. Druz, R. Kong, P. V Thomas, K. Wagh, T. Zhou, A.-J. Behrens, T. Bylund, C. W. Choi, J. R. Davison, I. S. Georgiev, M. G. Joyce, Y. Do Kwon, M. Pancera, J. Taft, Y. Yang, B. Zhang, S. S. Shivatare, V. S. Shivatare, C.-C. D. Lee, C.-Y. Wu, C. A. Bewley, D. R. Burton, W. C. Koff, M. Connors, M. Crispin, U. Baxa, B. T. Korber, C.-H. Wong, J. R. Mascola, P. D. Kwong, Trimeric HIV-1-Env structures define glycan shields from Clades A, B, and G. *Cell*. **165**, 813–26 (2016).

33. D. Sok, K. J. Doores, B. Briney, K. M. Le, K. L. Saye-Francisco, A. Ramos, D. W. Kulp, J. P. Julien, S. Menis, L. Wickramasinghe, M. S. Seaman, W. R. Schief, I. A. Wilson, P. Poignard, D. R. Burton, Promiscuous glycan site recognition by antibodies to the high-mannose patch of gp120 broadens neutralization of HIV. *Sci. Transl. Med.* **6**, 236ra63 (2014).

34. L. Cao, M. Pauthner, R. Andrabi, K. Rantalainen, Z. Berndsen, J. K. Diedrich, S. Menis, D. Sok, R. Bastidas, S.-K. R. Park, C. M. Delahunty, L. He, J. Guenaga, R. T. Wyatt, W. R. Schief, A. B. Ward, J. R. Yates, D. R. Burton, J. C. Paulson, Differential processing of HIV envelope glycans on the virus and soluble recombinant trimer. *Nat. Commun.* **9**, 3693 (2018).

35. D. Pinto, Y.-J. Park, M. Beltramello, A. C. Walls, M. A. Tortorici, S. Bianchi, S.

Jaconi, K. Culap, F. Zatta, A. De Marco, A. Peter, B. Guarino, R. Spreafico, E. Cameroni, J. B. Case, R. E. Chen, C. Havenar-Daughton, G. Snell, A. Telenti, H. W. Virgin, A. Lanzavecchia, M. S. Diamond, K. Fink, D. Veesler, D. Corti, *bioRxiv*, in press, doi:10.1101/2020.04.07.023903.

36. L. K. Pritchard, D. J. Harvey, C. Bonomelli, M. Crispin, K. J. Doores, Cell- and protein-directed glycosylation of native cleaved HIV-1 envelope. *J. Virol.* **89**, 8932–44 (2015).

37. T. Grant, A. Rohou, N. Grigorieff, CisTEM, user-friendly software for single-particle image processing. *eLife*. **7** (2018), doi:10.7554/eLife.35383.

38. P. Emsley, M. Crispin, Structural analysis of glycoproteins: Building N-linked glycans with coot. *Acta Crystallogr. Sect. D Struct. Biol.* **74**, 256–263 (2018).